Int. J. Heat Mass Transfer. Vol. 35, No. 10, pp. 2675–2682, 1992
Printed in Great Britain

0017–9310/92 $5.00 + 0.00

Transient heat and mass transfer of interacting vaporizing droplets in a linear array

HSUCHENG CHIANG and CLEMENT KLEINSTREUER†
Department of Mechanical and Aerospace Engineering, North Carolina State University, Raleigh, NC 27695-7910, U.S.A.

(*Received* 18 *March* 1991 *and in final form* 30 *September* 1991)

Abstract—A validated computer simulation model, based on an extended finite element software package, has been developed for the detailed analysis of colinear interacting vaporizing droplets in a heated air stream. The complete transport equations describing transient laminar axisymmetric fluid–particle flow with phase change have been solved for three closely-spaced *n*-octane fuel droplets and a free-stream ambient with $Re_0 = 100$, $T_\infty = 1000$ K and $p_\infty = 10$ atm. Of interest are the gas-phase temperatures and vapor concentrations with time, the transient interfacial phenomena and integral properties, such as $\overline{Nu}_g$, $\overline{Sh}_g$ and c_D, for each droplet. Comparisons with approximate analyses of three colinear monodisperse droplets and empirical studies for a solitary blowing sphere are included.

1. INTRODUCTION

TRANSIENT forced convection heat transfer between a heated gas stream and multiple evaporating droplets in a linear array is an important *base-case system* for droplet sprays and dense fluid–particle fields. Of interest is the analysis of the coupled nonlinear interfacial transport phenomena which largely determine practical integral properties such as total drag, vaporization rate and heat transfer coefficient of each interacting droplet. The present paper is a significant extension of our previous study of quasi-steady flow past constant-diameter droplets with prescribed liquid-phase vortex and constant droplet temperature [1].

Basic experimental and numerical studies of forced convection past a single vaporizing drop or a liquid sphere with surface mass transfer are well documented [2–7]. For example, Renksizbulut and Yuen [2] developed an empirical Nusselt number correlation $Nu = Nu(Re, B_H, Pr)$ for a porous sphere, representing an evaporating droplet. Numerical studies [3, 6, 7] expanded on their experiments and included drag correlations and the effects of variable gas-phase properties. Conner and Elghobashi [4] provided a finite difference solution of laminar flow ($Re \leqslant 100$) past a liquid sphere with surface blowing, and demonstrated its measurable influence on flow separation, drag coefficient, wake length, and the average Sherwood number.

Detailed multiple-particle investigations are typically restricted to low Reynolds number flows past two solid spheres or vaporizing droplets in tandem. For example, Zaprynov and Toshev [8] solved numerically the complete transport equations for steady axisymmetric thermal flow around a pair of spheres at $Re \leqslant 40$. Raju and Sirignano [9] considered two vaporizing droplets, one following the other with an initial Reynolds number of $Re_0 = 100$ for the leading droplet. In contrast, Kleinstreuer and Wang [10] used a relatively simple but sufficiently accurate, patched boundary-layer approach, utilizing detailed numerical correlations for the drag/interaction coefficients and temperature fields [11, 12] to analyse the dynamics of three interacting vaporizing fuel droplets on a one-dimensional trajectory. Relevant experimental work is still limited to flow visualization and measurements of the drag coefficients for two-sphere systems [13, 14] or for nonevaporating water drops on a two-dimensional trajectory [15]. At least *three* particles have to be considered for the evaluation of realistic interaction effects. Such minimum particle configurations are computationally efficient and set the stage for more generalized analyses.

2. ANALYSIS

2.1. *Governing equations*

Considering transient laminar axisymmetric flow of a heated incompressible fluid past three colinear, vaporizing droplets with initial heating and shear-stress induced internal circulation, the governing dimensionless equations are (cf. Fig. 1)

gas phase:

$$\nabla \cdot \mathbf{v}_g = 0 \tag{1}$$

$$\left(\frac{\partial}{\partial \tau} + \mathbf{v}_g \cdot \nabla\right)\mathbf{v}_g = -\nabla p_g + Re_g^{-1}\nabla^2 \mathbf{v}_g \tag{2}$$

$$\left(\frac{\partial}{\partial \tau} + \mathbf{v}_g \cdot \nabla\right) T_g = Pe_{h,g}^{-1}\nabla^2 T_g \tag{3}$$

$$\left(\frac{\partial}{\partial \tau} + \mathbf{v}_g \cdot \nabla\right) Y_g = Pe_{m,g}^{-1}\nabla^2 Y_g \tag{4}$$

† Author to whom correspondence should be addressed.

NOMENCLATURE

a	radius of droplet
B_H	heat transfer number, $c_p\Delta T/L$
c_D	drag coefficient
c_p	heat capacity; pressure drag coefficient
d	droplet diameter
d_{ij}	dimensionless interdroplet distances, d^*_{ij}/d^*_o
$\mathscr{D}$	diffusion coefficient
h	heat transfer coefficient
L	latent heat of vaporization
Le	Lewis number, Sc/Pr
M	molecular weight
p	pressure
Nu	Nusselt number, hd/k
Pr	Prandtl number, ν/α
Pe	Peclet number, $Re\ Pr$
R	radial cylindrical coordinate; gas constant
r	radial spherical coordinate
Re	Reynolds number, Ud/ν
Sc	Schmidt number, $\nu/\mathscr{D}$
Sh	Sherwood number, $hd/(\rho\mathscr{D})$
T	temperature
$\mathbf{v}$	velocity vector
u_n	normal or local blowing velocity
u_t	tangential velocity
u, v	velocity components
U	characteristic or free stream velocity
X	mole fraction
Y	mass fraction
Z	axial coordinate.

Greek symbols

α	thermal diffusivity
θ	spherical coordinate
ν	kinematic viscosity
ρ	density
τ	dimensionless time, tU/d^*_0
τ_s	surface shear stress.

Subscripts

a	air
b	surface blowing
bp	boiling point
D	total drag
F	friction
f	fuel
g	gas phase
h	heat transfer
i	index for particle spacing ($i = 1, 2$)
j	index for particle spacing ($j = i+1$)
k	index for particle identification ($k = 1, 2, 3$)
l	liquid phase
m	mass transfer
o	initial, reference
P	pressure
s	surface
T	thrust
∞	at infinity.

Superscripts

*	dimensional quantities.

and

liquid phase:

$$\nabla\cdot\mathbf{v}_l = 0 \tag{5}$$

$$\left(\frac{\partial}{\partial\tau}+\mathbf{v}_l\cdot\nabla\right)\mathbf{v}_l = -\nabla p_l + Re_l^{-1}\nabla^2\mathbf{v}_l \tag{6}$$

$$\left(\frac{\partial}{\partial\tau}+\mathbf{v}_l\cdot\nabla\right)T_l = Pe_{h,l}^{-1}\nabla^2 T_l \tag{7}$$

where

$$Re_o = Ud_o/\nu,\quad Pe_h = Ud_o/\alpha \quad\text{and}\quad Pe_m = Ud_o/\mathscr{D}. \tag{8a–c}$$

2.2. *Compatibility conditions*

Both phases are coupled via the interfacial conditions representing conservation of mass, momentum and energy. Specifically, continuous velocities, shear stress and temperature are required at the gas–liquid boundaries (cf. Fig. 1)

$$u_{t,g} = u_{t,l};\quad \tau_{s,g} = \tau_{s,l} \quad\text{and}\quad T_{s,g} = T_{s,l}. \tag{9a–c}$$

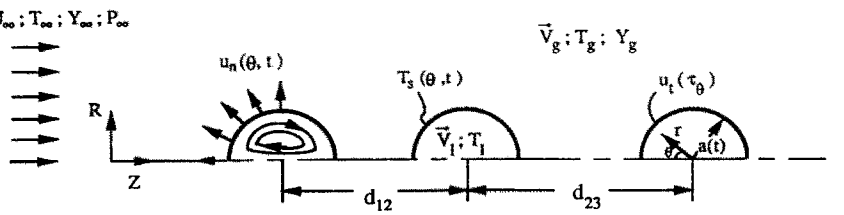

FIG. 1. System schematics and coordinates.

The normal interfacial velocity, i.e. the vapor blowing velocity, is proportional to the dimensionless diffusion mass flux

$$u_{n,g} = \frac{1}{1-Y_s} q''_{m,g} = -\frac{1}{1-Y_s} Pe_{m,g}^{-1} \left(\frac{\partial Y}{\partial r}\right)\bigg|_{r=a(\tau)} \tag{10}$$

where Y_s is the vapor concentration at the droplet surface assuming thermodynamic equilibrium

$$Y_s = \frac{M_f X_s}{M_f X_s + M_a(1-X_s)} \tag{11a}$$

where

$$X_s = \exp\left[\frac{L}{R}\left(\frac{1}{T_{bp}} - \frac{1}{T_s}\right)\right]. \tag{11b}$$

The heat transferred from the gas stream divides up into liquid droplet heating and latent heat of vaporization

$$q''_{h,l} = \frac{1}{\gamma}\left(q''_{h,g} - \frac{Lu_{n,g}}{c_{p,g}T_\infty}\right) \tag{12a}$$

where

$$\gamma = \frac{\rho_l c_{p,l}}{\rho_g c_{p,g}} \quad \text{and} \quad q''_{h,g} = -Pe_{h,g}^{-1}\frac{\partial T}{\partial r}\bigg|_{r=a(\tau)}. \tag{12b,c}$$

Assuming spherical droplets at all times, the decrease in droplet radius with time, or shrinkage, can be expressed as

$$\frac{da}{d\tau} = \frac{\rho_g}{2\rho_l}\int_0^\pi u_{n,g}\sin\theta\, d\theta. \tag{13}$$

Initially, at $\tau = 0$:

$$T_{g,l} = u_{g,l} = v_{g,l} = Y_g = 0. \tag{14a–d}$$

At the domain inlet

$$u_g = 1, \quad v_g = 0, \quad T_g = 1 \quad \text{and} \quad Y_g = 0. \tag{15a–d}$$

Because of symmetry, all gradients at the centerline ($R = 0$) are equal to zero. The extent of the computational domain, being a function of the free-stream Reynolds number [1], is large enough so that all appropriate outer boundary and outlet gradients are identically zero (cf. Fig. 2(a)).

2.3. *Averaged interfacial properties*

In general, averaged surface properties, such as heat flux, vapor flux, shear stress, etc., are evaluated by integration of the local variable, namely

$$\bar{g} = \frac{1}{2}\int_0^\pi g(\theta)\sin\theta\, d\theta. \tag{16}$$

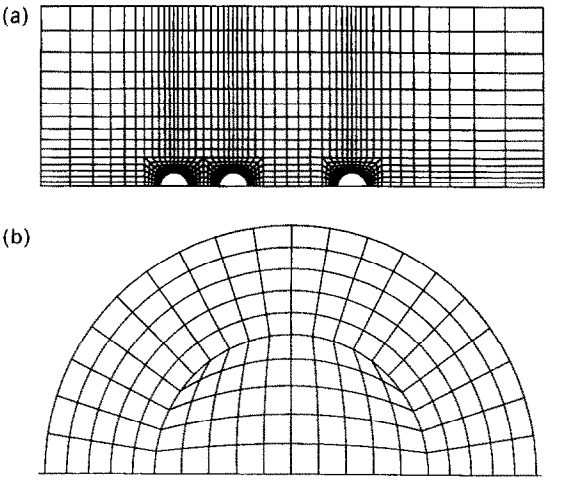

FIG. 2. (a) Gas-phase domain mesh for $Re_0 = 100$. (b) Liquid-phase domain mesh.

Thus, the gas-phase, surface-averaged Nusselt number and Sherwood number can be calculated as

$$\overline{Nu}_g = \frac{hd^*(t)}{k} = \frac{2a(\tau)}{1-\bar{T}_s}(\bar{q}''_{h,g}\, Pe_{h,g}) \tag{17}$$

and

$$\overline{Sh}_g = \frac{hd^*(t)}{\mathscr{D}} = \frac{2a(\tau)}{\bar{Y}_s}(\bar{q}''_{m,g}\, Pe_{m,g}). \tag{18}$$

The total drag on each vaporizing interacting droplet is due to friction drag, pressure drag and, usually negligible, thrust drag

$$c_F = -4\int_0^\pi \tau_{r\theta}|_{r=a(\tau)} \sin^2\theta\, d\theta \tag{19a}$$

$$c_P = 2\int_0^\pi p|_{r=a(\tau)} \sin 2\theta\, d\theta \tag{19b}$$

$$c_T = 4\int_0^\pi (u_n^2\cos\theta - 2u_n u_t \sin\theta)\sin\theta\, d\theta. \tag{19c}$$

3. NUMERICAL SOLUTION METHOD

The governing equations (1)–(7), subject to the conditions (9)–(15) are solved using a widely accepted finite-element software package [16]. Actually, the penalty function approach is used where the continuity requirement is weakened by replacing equation (1) with $\nabla\cdot\mathbf{v} = \varepsilon p$, where the penalty parameter ε is very small, that is, $\varepsilon = \mathcal{O}(10^{-6})$. The elements chosen are isoparametric quadrilaterals with nine nodes. Biquadratic shape functions are selected for approximating velocity, temperature and vapor concentration profiles, whereas the pressure is given by discontinuous linear shape functions [17]. A representative global mesh and a sample mesh for the gas–liquid interfacial regions are shown in Figs. 2(a) and (b), respectively. Typically, a total of 6000 nodal points, where $\Delta\theta = 4^\circ$ on the droplet surface, are needed.

Very small elements are placed at the interface and large elements near the domain boundaries. A smooth transition from fine to coarse mesh regions has been achieved. The overall mesh size has been obtained in accordance with the boundary conditions by trial and error. Specifically, the location of the upper domain boundary is about $12a$ for $Re = 100$, where a is the droplet radius. Independence of the simulation results from the mesh density has been successfully tested based on repeat calculations with finer meshes.

Computations for the *coupled* transient two-phase flow variations are started with the developed gas-phase parameters ($\mathbf{v}_g$, T_g, Y_g) in place and the droplets fixed at prescribed initial temperatures. Thus, the gas-side shear stress, diffusion heat flux and mass flux are used as boundary conditions for solving the liquid-phase equations (5)–(7). Then the normal and tangential surface velocities, surface temperature and vapor concentration are calculated and used as input for solving the gas-phase equations (1)–(4).

A quasi-Newton algorithm is employed for solving the nonlinear equations with a reformation of the Jacobian matrix every five steps. Actually, a slower but more robust successive substitution method is applied for the first three steps to bring the solution within the radius of convergence of the quasi-Newton scheme which is invoked subsequently. This procedure is especially beneficial for the liquid region because its Neumann-type boundary conditions may propagate errors with time. Typically, convergence is obtained within eight iterations when $\varepsilon = |(T_\zeta^{i+1} - T_\zeta^i)/T_\zeta^i| \leqslant 10^{-4}$.

With the initial dimensionless droplet radius being $a_0 = 0.5$, shrinkage (cf. equation (11)) is evaluated after each (converged) time step, and a locally refined mesh is implemented. The computations proceed until about 20% of the droplet mass has been evaporated. A complete run for, say, $Re_0 = 100$, $T_\infty = 1000$ K and $T_0 = 300$ K, takes about 8 h on a CRAY Y-MP. With the given post-processing capabilities, wall heat flux calculations as well as plots of velocity vector fields, pressure surfaces, vorticity contours, isotherms and temperature surfaces can be conveniently executed.

4. RESULTS AND DISCUSSION

The present study, in an extension to the results of Chiang and Kleinstreuer [1], focuses on the transient interfacial transport phenomena of three interacting vaporizing droplets in a laminar axisymmetric heated gas stream. For this base case study, a representative free stream Reynolds number of $Re_0 = 100$ and fixed droplet distances of $d_{12} = 2$ and $d_{23} = 4$ are selected. Other model input data are summarized in Table 1. The accuracy of the computer code, relative to experimental and numerical results for simpler problems, has been successfully documented in several papers [1, 11, 12, 18]. Thus, model validation is only indirectly addressed in comparisons with results and correlations given by Chiang and Kleinstreuer [18], Renksizbulut and Yuen [2, 3], and Haywood *et al.* [6].

Table 1. Input data set [20]

density ratio, ρ_l/ρ_g	209.2
capacity ratio, $c_{p,l}/c_{p,g}$	1.94
viscosity ratio, μ_l/μ_g	21.44
gas phase Prandtl number, Pr_g	0.72
gas phase Schmidt number, Sc_g	3.26
liquid phase Prandtl number, Pr_l	10.0
gas phase Reynolds number, Re_g	100.0
latent heat, $L/c_{p,g}$ (K)	267.1
droplet diameter, d_0 (μm)	50.0
free stream temperature, T_∞ (K)	1000.0
boiling point of fuel, T_{bp} (K)	508.0
droplet initial temperature, T_0 (K)	300.0
ambient pressure, p_∞ (atm)	10.0
molecular weight, M_f (*n*-octane)	114.0

4.1. *Contour plots*

Figures 3(a)–(c) and 4(a)–(c) show the temporal evolution ($\tau = 10$, 100, 300) of isotherms and vapor concentration contours, respectively. *Liquid-phase* heating is first due to conduction until internal droplet circulation ($\tau > 100$) makes convection heat transfer dominant. However, decreasing interfacial shear stress ($\tau > 200$) weakens internal circulation and conduction heat transfer gradually takes over again. The effect of mass transfer is most visible in the shrinking of the first droplet (cf. Figs. 4(a) and (c)). The *gas-phase* contours illustrate the thickening of the thermal (Figs. 3(a)–(c)) and concentration (Figs. 4(a)–(c)) boundary layers because of increasing surface vapor blowing and decreasing droplet Reynolds numbers. The patterns between isotherms and concentration contours differ significantly because of the large discrepancy between the Schmidt number ($Sc = 1.2$–4 for fuel vapor diffusion) and Prandtl number ($Pr = 0.7$–1.0 for gas phase). Hence, the resulting Lewis number ($Le = Sc/Pr$), usually set equal to unity, is an important indicator for droplet vaporization. Droplets 2 and 3 vaporize much slower when compared to droplet 1 because the fuel vapor is convected downstream, enveloping the trailing droplets and reducing mass transfer significantly.

4.2. *Averaged surface properties*

Based on equation (16), the surface-averaged interfacial velocities as well as temperatures and concentrations are shown for the three interacting vaporizing droplets in Fig. 5 and Fig. 6, respectively. At first, $0 \leqslant \tau \leqslant 40$, large shear stresses accelerate the liquid near the droplet surface resulting in peak tangential velocities (cf. Fig. 5) which then quickly decrease because of the combined effects of increasing surface blowing (cf. Figs. 5 and 6) and rapid decrease in interfacial shear stress. It has to be noted that the interfacial velocities for the third droplet are higher than for the second droplet because droplet 2 is here directly in the wake of the leading droplet while droplet 3, a significant distance downstream, experiences

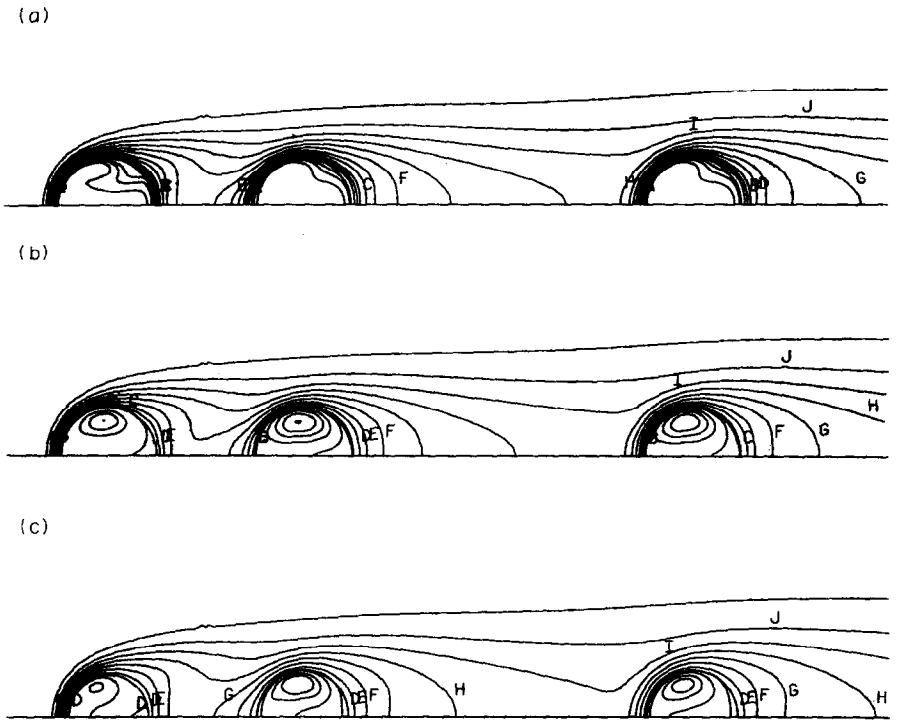

FIG. 3. (a) Isotherms of interacting vaporizing droplets at $\tau = 10$ for $Re_0 = 100$, $d_{12} = 2$ and $d_{23} = 4$ (A = 0.38, B = 0.41, C = 0.44, D = 0.49, E = 0.54, F = 0.61, G = 0.68, H = 0.75, I = 0.82, J = 0.89, K = 0.96). (b) Isotherms of interacting vaporizing droplets at $\tau = 100$ for $Re_0 = 100$, $d_{12} = 2$ and $d_{23} = 4$ (A = 0.38, B = 0.41, C = 0.44, D = 0.49, E = 0.54, F = 0.61, G = 0.68, H = 0.75, I = 0.82, J = 0.89, K = 0.96). (c) Isotherms of interacting vaporizing droplets at $\tau = 300$ for $Re_0 = 100$, $d_{12} = 2$ and $d_{23} = 4$ (A = 0.38, B = 0.41, C = 0.44, D = 0.49, E = 0.54, F = 0.61, G = 0.68, H = 0.75, I = 0.82, J = 0.89, K = 0.96).

more of a solitary-droplet impact. Figure 6 confirms our earlier observation [1] that for a dense droplet spray (i.e. $d_{ij} < 6$), *heat transfer* values for the leading droplet are overwhelming and those for the following droplets are lower and very similar. When compared with boundary-layer studies (e.g. ref. [10] or [19]) where $Le \approx 1$ was assumed, the present results indicate higher surface temperatures and vapor concentrations. For the heavy fuel considered in this analysis (cf. Table 1), mass diffusion is rather weak when compared to thermal diffusion leading to larger interfacial vapor concentrations and higher surface temperatures because most of the incoming energy is utilized in liquid droplet heating.

Figures 7 and 8 depict the gas-phase Nusselt number and Sherwood numbers with time for each droplet as well as empirical correlations (cf. equations (17) and (10) as well as refs. [2, 6]). The R&Y correlation [2] for the transient Nusselt number of a single evaporating (porous) sphere is close to $\overline{Nu}_g(\tau)$ for the first droplet except during the initial stage, $0 \leqslant \tau < 100$, when large surface tangential velocities increase interfacial heat transfer. Overall, upstream interaction effects do not interfere significantly with the heat transfer of the leading droplet. The trailing droplets are strongly affected by the wake of droplet 1; again with $\overline{Nu}_{g,3} > \overline{Nu}_{g,2}$ because of the interdroplet distances chosen. The approximate study [18], assuming uniform fluid injection at constant surface temperature for porous spheres, predicts acceptable heat transfer coefficients except for the leading droplet which exhibits highly nonuniform surface blowing velocities as time progresses. Effects of droplet interaction, initial heating and shrinking are more pronounced for surface mass transfer (cf. Fig. 8). This explains the prevailing differences between $\overline{Sh}_g$ of the empirical correlation and that of the first droplet. At a time level of about $\tau = 60$, a somewhat uniform trend in vapor and heat transfer mechanism is established (cf. Figs. 5–8) and the gas-phase Sherwood numbers are approximately the same for all three droplets.

Figure 9 depicts droplet radius reduction with time for the three droplets due to phase change. As expected, the nonlinear rate of shrinkage for the leading droplet is measurably higher than for the trailing droplets, and for the present droplet configuration, the third droplet evaporates faster than the second droplet.

The transient drag coefficients for each droplet (cf. equation (19)) are shown in Fig. 10 and compared with an empirical correlation [3] for a single blowing sphere, which does not incorporate interaction effects,

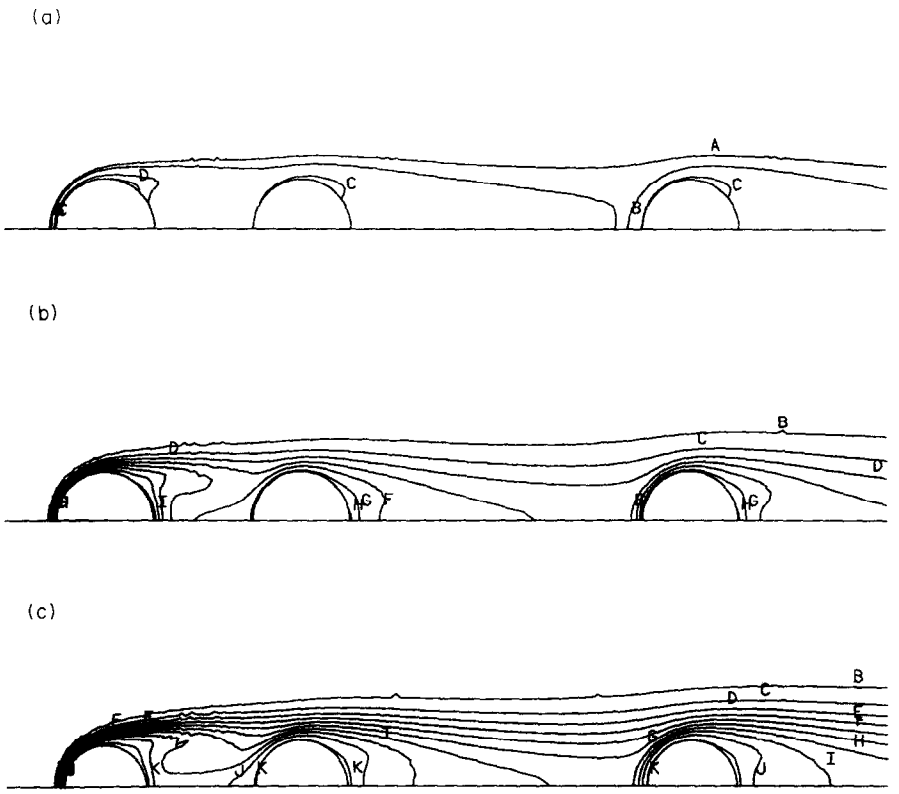

FIG. 4. (a) Vapor concentration contours of interacting vaporizing droplets at $\tau = 10$ for $Re_0 = 100$, $d_{12} = 2$ and $d_{23} = 4$ (A = 0.03, B = 0.05, C = 0.1, D = 0.15, E = 0.2, F = 0.3, G = 0.4, H = 0.5, I = 0.6, J = 0.7, K = 0.8, L = 0.9). (b) Vapor concentration contours of interacting vaporizing droplets at $\tau = 100$ for $Re_0 = 100$, $d_{12} = 2$ and $d_{23} = 4$ (A = 0.03, B = 0.05, C = 0.1, D = 0.15, E = 0.2, F = 0.3, G = 0.4, H = 0.5, I = 0.6, J = 0.7, K = 0.8, L = 0.9). (c) Vapor concentration contours of interacting vaporizing droplets at $\tau = 300$ for $Re_0 = 100$, $d_{12} = 2$ and $d_{23} = 4$ (A = 0.03, B = 0.05, C = 0.1, D = 0.15, E = 0.2, F = 0.3, G = 0.4, H = 0.5, I = 0.6, J = 0.7, K = 0.8, L = 0.9).

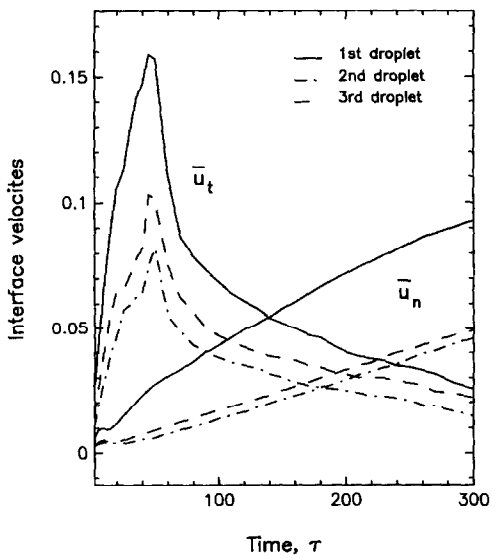

FIG. 5. Transient surface-averaged interfacial velocities for three interacting vaporizing droplets at $Re_0 = 100$ ($d_{12} = 2$ and $d_{23} = 4$).

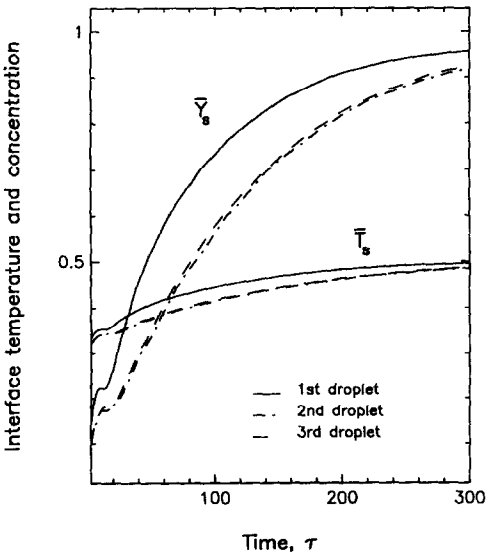

FIG. 6. Transient surface-averaged interfacial temperatures and vapor concentrations for three interacting vaporizing droplets at $Re_0 = 100$ ($d_{12} = 2$ and $d_{23} = 4$).

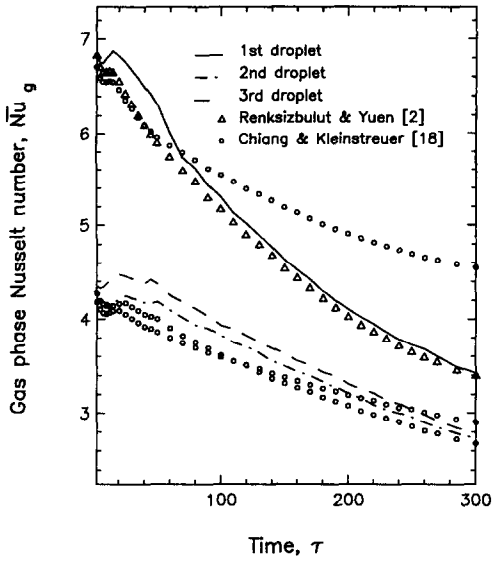

FIG. 7. Comparison between transient surface-averaged interfacial temperatures and vapor concentrations for gas-phase Nusselt numbers for three interacting vaporizing droplets ($Re_0 = 100$, $d_{12} = 2$, $d_{23} = 4$) and a solitary blowing sphere (correlations [2] and numerical results [18]).

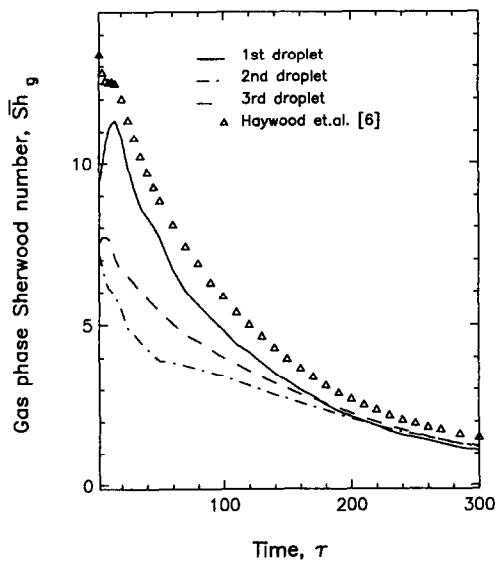

FIG. 8. Comparison between transient surface-averaged interfacial temperatures and vapor concentrations for gas-phase Sherwood numbers for three interacting vaporizing droplets ($Re_0 = 100$, $d_{12} = 2$, $d_{23} = 4$) and a solitary blowing sphere (Haywood *et al.* [6]).

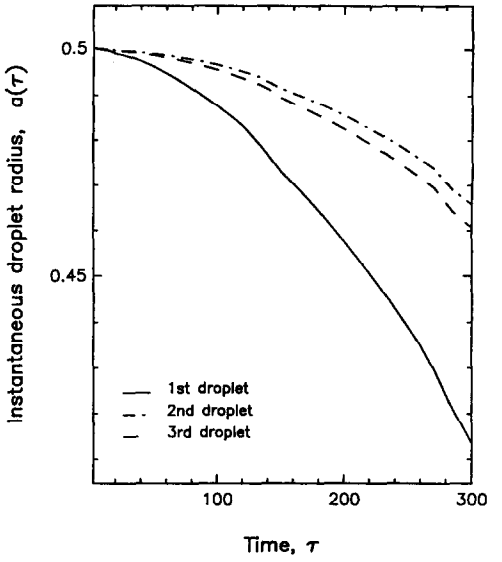

FIG. 9. Spherical droplet shrinking with time ($Re_0 = 100$, $d_{22} = 2$ and $d_{23} = 4$).

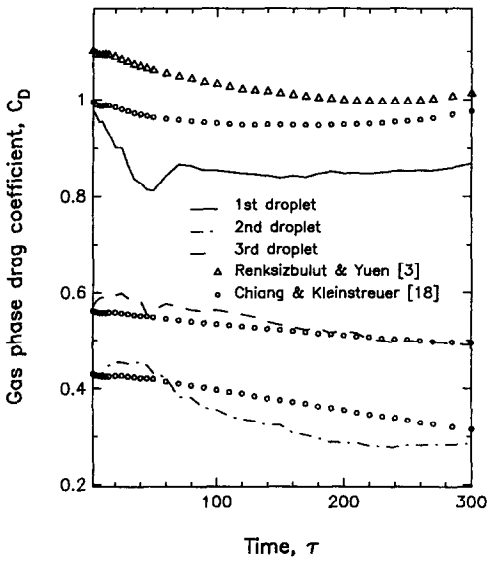

FIG. 10. Transient drag coefficients for three interacting droplets ($Re_0 = 100$, $d_{12} = 2$, $d_{23} = 4$) and a solitary porous sphere with blowing (Renksizbulut and Yuen [3] and Chiang and Kleinstreuer [18]).

variable Lewis numbers, and internal circulation. Again, the approximate analysis of blowing spheres [18] predicts correct c_Ds for all particles at $\tau = 0$ but then differs from the present results for the first droplet because of the effects of slip velocity and non-uniform blowing not considered by Chiang and Kleinstreuer [18]. While the large tangential velocity first reduces the friction drag ($\tau < 50$), the increase in surface blowing balances via a higher pressure drag the surface slip effect and the total drag coefficient of the first droplet stays about 15% below that of a solitary blowing sphere thereafter. The transient drag coefficient of the second droplet is significantly lower and less uniform than that of the third droplet. Thus, coalescence between droplets 1 and 2 is imminent and droplet 3 may be further separated.

Acknowledgements—This work has been supported in part by the Department of Energy, Office of Basic Energy Science, grant No. DE-FG05-87ER13728. The support of the North Carolina Supercomputing Center (NCSC) under an

Advanced Computing Resources Grant from the State of North Carolina is greatly appreciated.

REFERENCES

1. H. Chiang and C. Kleinstreuer, Convection heat transfer of co-linear interacting droplets with surface mass transfer, *Int. J. Heat Fluid Flow* **12**, 233–239 (1991).
2. M. Renksizbulut and M. C. Yuen, Experimental study of droplet evaporation in a high-temperature air stream, *J. Heat Transfer* **105**, 384–388 (1983).
3. M. Renksizbulut and M. C. Yuen, Numerical study of droplet evaporation in a high-temperature stream, *J. Heat Transfer* **105**, 389–397 (1983).
4. J. M. Conner and S. E. Elghobashi, Numerical solution of laminar flow past a sphere with surface mass transfer, *Numer. Heat Transfer* **12**, 57–82 (1987).
5. G. Ryskin, Heat or mass transfer from a moving drop—some approximation relations for the Nusselt number, *Int. Commun. Heat Mass Transfer* **14**, 741–749 (1987).
6. R. J. Haywood, R. Nafziger and M. Renksizbulut, A detailed examination of gas and liquid phase transient processes in convective droplet evaporation, *J. Heat Transfer* **111**, 495–502 (1989).
7. C. H. Chiang, M. S. Raju and W. A. Sirignano, Numerical analysis of convecting vaporizing fuel droplet with variable properties, AIAA Paper 89-0834 (1989).
8. Z. D. Zaprynov and E. T. Toshev, Hydrodynamics and heat transfer around two separated spherical particles, *Proc. 8th Int. Conf. on Heat Transfer*, San Francisco, Vol. 5, pp. 2549–2553 (1986).
9. M. S. Raju and W. A. Sirignano, Interaction between two vaporizing droplets in an intermediate Reynolds number flow, *Physics Fluids A* **2**, 1780–1796 (1990).
10. C. Kleinstreuer and T.-Y. Wang, Approximate analysis of interacting vaporizing fuel droplets, *Int. J. Multiphase Flow* **16**, 295–304 (1990).
11. R. S. Ramachandran, C. Kleinstreuer and T.-Y. Wang, Forced convection heat transfer of interacting spheres, *Numer. Heat Transfer, Part A* **15**, 471–487 (1989).
12. R. S. Ramachandran, T.-Y. Wang, C. Kleinstreuer and H. Chiang, Laminar flow past three closely-spaced monodisperse spheres or nonevaporating drops, *AIAA J.* **29**, 43–45 (1991).
13. P. N. Rowe and G. A. Henwood, Drag forces in a hydraulic model of a fluidized bed—Part I, *Trans. Inst. Chem. Engrs* **39**, 43–56 (1961).
14. Y. Tsuji, Y. Morikawa and K. Terashima, Fluid-dynamic interaction between two spheres, *Int. J. Multiphase Flow* **8**, 71–82 (1982).
15. J. A. Mulholland, R. K. Srivastava and J. O. L. Wendt, Influence of droplet spacing on drag coefficient in non-evaporating monodisperse streams, *AIAA J.* **26**, 1231–1237 (1988).
16. M. S. Engelman, *FIDAP 5.0 Manuals*, Vols 1–3. FDI, Evanston, IL (1990).
17. C. Cuvelier, A. Segal and A. A. Van Steenhoven, *Finite Element Methods and Navier–Stokes Equations*. D. Reidel, Dordrecht, Holland (1986).
18. H. Chiang and C. Kleinstreuer, Laminar flow past co-linear spheres with fluid injection, *ASME J. Fluids Engng* **113**, 176–182 (1991).
19. C. Kleinstreuer, H. Chiang and T.-Y. Wang, Mathematical modeling of interacting vaporizing fuel droplets. In *Proceedings 1989 NHT Conf. HTD* (Edited by R. K. Shah), Vol. 106, pp. 469–478. ASME, New York (1989).
20. C. H. Chiang and W. A. Sirignano, Numerical analysis of interacting, convecting, vaporizing fuel droplets with variable properties, AIAA Paper 90-0357 (1990).

TRANSFERT VARIABLE DE CHALEUR ET DE MASSE DE GOUTTELETTES QUI SE VAPORISENT DANS UN ARRANGEMENT LINEAIRE

Résumé—Un modèle validé de simulation numérique a été développé pour l'analyse détaillée de gouttelettes en intéraction qui se vaporisent dans un écoulement d'air chaud. Les équations complètes de transport qui décrivent l'écoulement laminaire axisymétrique fluide-particules avec changement de phase ont été résolues pour trois gouttelettes de *n*-octane peu espacées et un écoulement libre ambiant avec $Re_0 = 100$, $T_\infty = 1000$ K et $p_\infty = 10$ atm. On considère les températures de la phase gazeuse et les concentrations de vapeur avec le temps, le phénomène interfacial variable et les propriétés intégrales telles que $\overline{Nu}_g$, $\overline{Sh}_g$ et c_D pour chaque gouttelette. On inclut des comparaisons avec des analyses approchées de trois gouttelettes colinéaires monodispersées et des études empiriques pour une sphère solitaire.

INSTATIONÄRER WÄRME- UND STOFFTRANSPORT VON WECHSELWIRKENDEN VERDAMPFENDEN TROPFEN IN LINEARER ANORDNUNG

Zusammenfassung—Für die detaillierte Analyse wechselwirkender verdampfender Tropfen in einem beheizten Luftstrom wird ein validiertes Simulationsmodell entwickelt, das auf einem umfangreichen Finite-Elemente Softwarepaket basiert. Die vollständigen Transportgleichungen für die instationäre laminare achsensymmetrische Fluid-Partikelströmung mit Phasenwechsel wird für drei dichtgepackte *n*-Oktan-Brennstofftröpfchen und eine Freistromumgebung mit $Re_0 = 100$, $T_\infty = 1000$ K und $p_\infty = 10$ atm gelöst. Von Interesse sind die zeitlichen Verläufe der Temperatur der Gasphase und der Konzentration des Dampfes, die transienten Grenzflächenphänomene und die integralen Eigenschaften jedes Tropfens, wie z. B. $\overline{Nu}_g$, $\overline{Sh}_g$ und c_D. Die vorgestellten Ergebnisse werden mit Näherungsuntersuchungen an drei kolinearen monodispersen Tropfen und mit empirischen Untersuchungen an einer einzelnen angeströmten Kugel verglichen.

НЕСТАЦИОНАРНЫЙ ТЕПЛО- И МАССОПЕРЕНОС ВЗАИМОДЕЙСТВУЮЩИХ ИСПАРЯЮЩИХСЯ КАПЕЛЬ, РАСПОЛОЖЕННЫХ ЛИНЕЙНО

Аннотация—На основе расширенного комплекта программного обеспечения с использованием метода конечных элементов разработана модель для детального анализа обтекания линейно расположенных взаимодействующих испаряющихся капель нагретым потоком воздуха. Получены решения полных уравнений переноса, описывающих нестационарное ламинарное осесимметричное течение жидкости и частиц при наличии фазового перехода для трех близко расположенных капель н-октанового топлива с параметрами обтекающей среды $Re_0 = 100$, $T_\infty = 1000$ K и $p_\infty = 10$ атм. Предствлет интерес изменение температур газообразной фазы и концентраций пара со временем, нестационарные процессы на границе раздела и такие интегральные характеристики как $\overline{Nu}_g$, $\overline{Sh}_g$ и c_D для каждой капли. Проводится сравнение приближенного анализа для трех монодисперсных линейно расположенных частиц и эмпирических результатов для одиночной обтекаемой сферы.